Chapter 3

Materials, methods, and characterization techniques

This chapter encompasses the following components: materials required, methods of synthesis of the samples, fabrication of electrodes, and characterization tools and techniques. Polyaniline (PANI) was synthesized by the chemical-oxidative polymerization (COP) route. Activated carbon was derived from coconut shells through pyrolysis, whereas all the binary metal oxides (copper ferrite, cobalt ferrite, and copper cobaltite) were synthesized using the sol-gel combustion technique.

PANI was chosen due to its simplicity and cost-effectiveness in chemical synthesis, its desirable flexibility, properties like chemical and environmental stability, and high conductivity when compared to other conducting polymers like polypyrrole, polythiophene etc. [207]. Extensive research has been conducted on transition metal oxides, such as cobalt oxide, copper oxide, iron oxide, etc., for supercapacitor applications. In this study, we have specifically selected bimetallic oxides like copper cobaltite (combination of Cu and Co), cobalt ferrite (Co and Fe), and copper ferrite (Cu and Fe) to harness the advantages of multiple oxidation states (from both metals) in a single compound. Further, the utilization of agro-waste to produce activated carbon materials is a sustainable methodology broadly used for different applications. Significant air pollution has resulted from agro-waste disposal in landfills or incineration in open areas, which has become a serious concern for researchers. Coconut shells are excellent candidates for activated carbon resources as they are inexpensive and renewable agricultural wastes [208]. India in particular, is the largest producer of coconuts, with approximately 20,000 million nuts produced in the year 2020. The consumption of coconuts has further increased post the covid pandemic due to the recognized health benefits of coconut water. Therefore, efficient and economical conversion technology needs to be developed to eliminate the waste disposal problem contributing to global warming. This approach not only minimizes waste but also utilizes it for energy storage applications [209].

The material characterization involved several techniques, including X-ray diffraction (XRD), Fourier transforms infrared spectroscopy (FTIR), X-ray photoelectron spectroscopy (XPS), Field emission scanning electron microscopy (FESEM), Energy-dispersive X-ray spectroscopy (EDS), and Transmission electron microscopy (TEM). These techniques were employed to examine the structural, chemical, and morphological properties of materials. Further, cyclic voltammetry (CV) was used to analyze the electrochemical behaviours and redox processes, charge-discharge (CD) measurements were performed to evaluate the energy storage capacity and charge storage efficiency. Additionally, electrochemical impedance spectroscopy (EIS) was employed to investigate charge transfer resistance of the fabricated elecrodes.

3.1 Materials required:

Aniline monomer, conducting silver adhesive paste, 2-propanol, Nafion binder, and Toray carbon paper were procured from Alfa Aesar, Thermo Fisher Scientific, United States. Ammonium persulfate (APS), para-toluene sulfonic acid (PTSA), copper nitrate, iron nitrate, cobalt nitrate, and glycine were purchased from Sigma Aldrich Chemicals Pvt Ltd. All the materials were analytical grade (ACS grade) and did not require further purification. All the experiments were performed at 25 °C temperature, and double distilled water served as a solvent. The chemical properties of the chemical compounds have been detailed in Table 3.1. Since aniline monomer is present in liquid form, the mole ratio calculations were done based on its specific gravity which is 1.021 g/mL.

Table 3.1: Specifications of the chemical compounds

Name	Chemical formulae	Molar mass (g/mol)	Purity (%)
Aniline monomer	C_6H_7N	93.13	≥ 99.5

PTSA	$C_7H_8O_3S.H_2O$	190.22	≥ 98.5
APS	$(NH_4)_2S_2O_8$	228.2	≥ 98.0
Copper nitrate	$Cu(NO_3)_2.3H_2O$	241.6	≥ 99.0
Ferric nitrate	$Fe(NO_3)_3.9H_2O$	404	≥ 99.0
Cobalt nitrate	$Co(NO_3)_2.6H_2O$	291.04	≥ 99.0
glycine	$C_2H_5NO_2$	75.07	> 99.0

3.2 Synthesis of polyaniline (PANI):

Polyaniline (PANI) was synthesized from aniline monomer (AN) by the chemical oxidative polymerization reaction (COP) technique. Ammonium persulfate (APS) was used as an initiator and oxidant. Paratoluene sulfonic acid (PTSA) was used as a doping agent. Solution 1 was made of PTSA (0.05 mol), while the other solution was of APS (0.125 mol) dissolved in double-distilled water. These solutions were cooled below 5 °C using an ice bath on the magnetic stirrer. The second step involved the addition of aniline monomer dropwise into the previously prepared PTSA solution. The resulting solution was stirred continuously to prevent precipitation and maintain homogeneity. Care was taken to ensure a slow and controlled addition on aniline to avoid a rapid temperature rise. The previously prepared APS solution was added very slowly to the aniline-PTSA solution to initiate the polymerization reaction. The polymerization process thus started, which is exothermic; therefore, a very slow rate of addition of APS was maintained to prevent any abrupt rise in temperature [210]. Initially, the solution was brownish in color; eventually, a dark green precipitate was formed with the complete addition of APS solution. The resulting mixture (precipitate) was stirred for 1 hour, and kept in a refrigerator overnight, followed by vacuum filtration, washing several times, and vacuum

drying at 70 °C for 8 hours [211]. The dried samples were ground to powder form and stored at normal conditions for further use. It should be noted that adding aniline to PTSA instantly would result in the formation of a low-grade PANI. Similarly, a quick addition of APS solution to the aniline-PTSA solution would result in the uncontrollable burning of the sample. A schematic diagram and experimental set-up for the synthesis of polyaniline have been shown in figure 3.1 (a) and (b), and its flow diagram has been shown in figure 3.2.

(a)

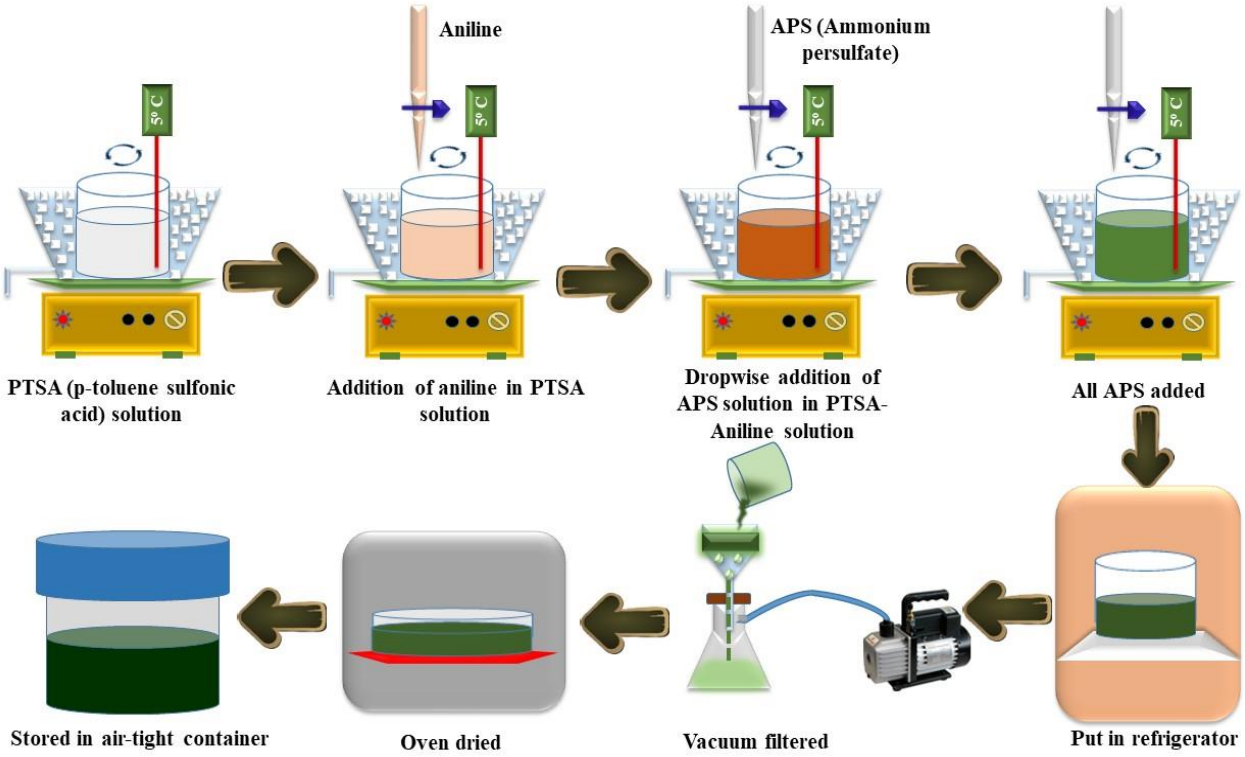

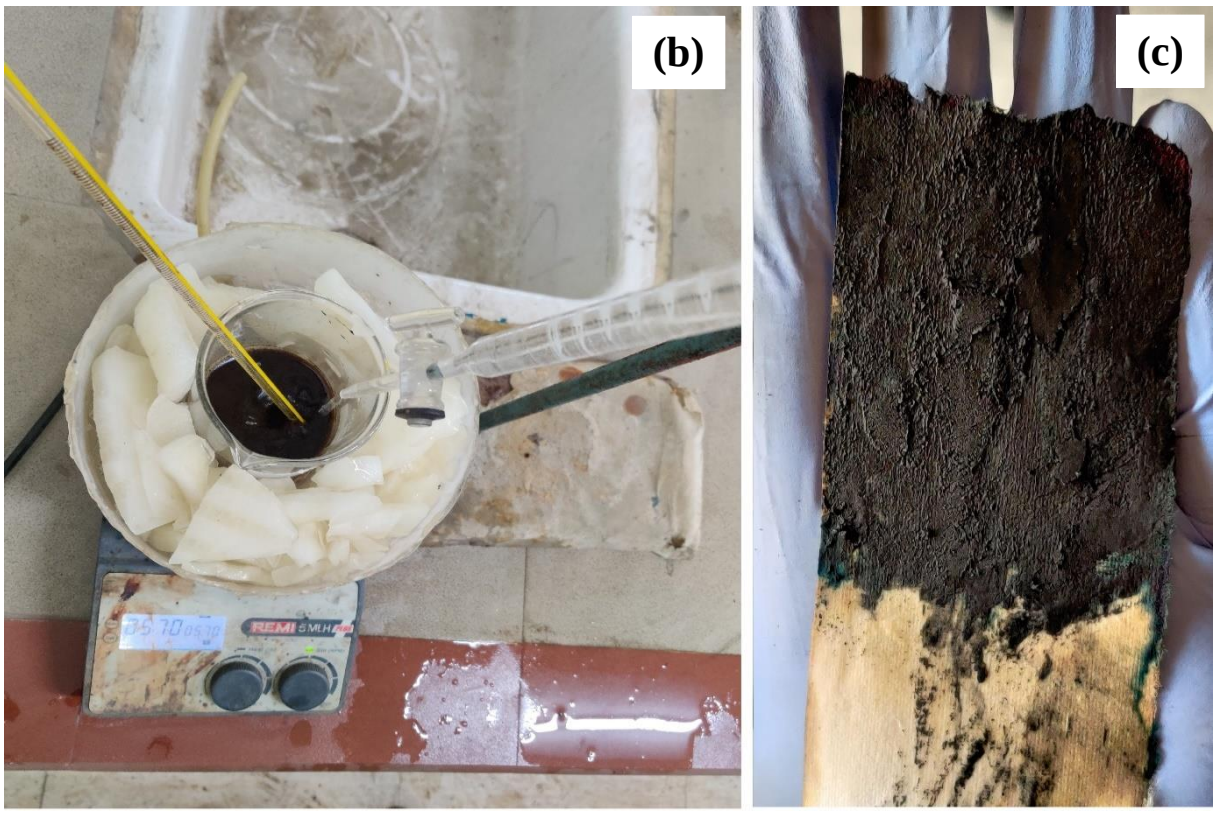

Fig 3.1: (a) Schematic diagram, (b) experimental set-up and (c) dark green precipitate formed during the synthesis of polyaniline

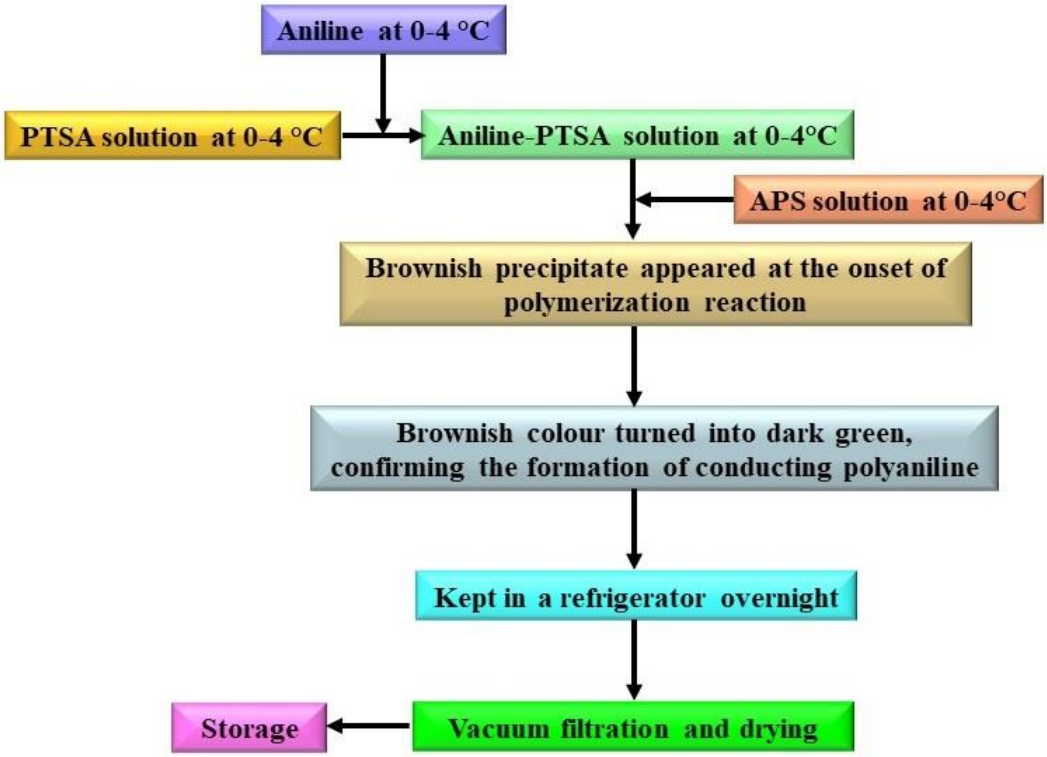

Fig 3.2: Flow diagram for synthesis of polyaniline

3.3 Synthesis of binary metal oxides

Solution combustion technique was employed to synthesize three different binary metal oxides, namely copper cobaltite (CuCo), cobalt ferrite (CoF), and copper ferrite (CuF). This technique was chosen owing to its numerous advantages such as simplicity of set-up and its availability in laboratory, cost effectiveness, absence of complex processing steps therefore no expensive equipment is required, lower environmental impact, better scalability for large scale production, involvement of self-propagating fast reaction which decreases synthesis time, lower energy requirements, high-purity products due to high reaction temperature which can volatile the impurities, and flexibility of adjustment of synthesis parameters for fine-tuning the properties. Further, the solution combustion method possess various features that distinguish it from other techniques. In solution combustion processes, the majority of heat is supplied by oxidation of organic fuel components and the target is mainly metals or metal oxides. Therefore, as a result of large amounts of gaseous byproducts, a considerable expansion of the solid product takes place and a rapid drop in temperature after the reaction, makes the solid product porous and thoroughly dispersed. The kinetics of a reaction, which involves the rate at which a system reaches equilibrium, is crucial from a practical standpoint. It determines the characteristic temperature and processing time needed for synthesis, which subsequently influences the formation of products with specific properties. One of the benefits of solution combustion technique is its capability to produce nanoscale powders with the desired crystal structure in a single step which is more suitable for large scale production [261-262].

The co-precipitation technique, on the other hand utilizes careful control over temperature and requires additional equipment (such as oil bath) for the same and simultaneous pH control thereby introducing complexity in the process of synthesis for binary metal oxides. Further,

additional steps are required in processing such as centrifugation, washing and drying followed by calcination thereby adding more constraints to the process as compared to a single step combustion method. In the case of sol-gel technique, although the process is simple for synthesis of binary metal oxides, the time required for reaction is fairly high (upto 24 hours) and requires a separate source of heat throughout the process and the heat of combustion is provided by an external source as opposes to oxidation in the case of solution combustion process [263].

To synthesize copper cobaltite ($CuCo_2O_4$), cobalt nitrate (0.02 mol) and copper nitrate (0.01) were mixed in 400 mL DDW with the help of a magnetic stirrer to get a uniform suspension. Then, 0.045 mol glycine was added to the mixture, and the temperature was raised to 75-80° C. After 8 hrs, a red-hot flame erupted, and as a consequence, copper cobaltite particles were obtained by following the chemical reaction (3.1). The CuCo particles were crushed to a fine powder in a mortar pestle, and calcined at 600° C for 6 hrs [212]. The synthesized particles were stored for further use.

$$9\ Cu(NO_3)_2.3\ H_2O + 18\ Co(NO_3)_2.6\ H_2O + 28\ C_2H_5NO_2 \rightarrow 9\ CuCo_2O_4 + 205\ H_2O + 56\ CO_2 + 41\ N_2 \quad (3.1)$$

In the synthesis of cobalt ferrite ($CoFe_2O_4$), ferric nitrate monohydrate, and cobalt nitrate hexahydrate were used as raw material along with glycine as fuel according to chemical reaction (3.2).

Ferric nitrate (0.02 mol) and cobalt nitrate (0.01 mol) were dissolved in a beaker containing 400 mL double distilled water. A magnetic stirrer was employed to ensure the formation of homogenous suspension. Glycine (0.045 mol) fuel was added with continuous stirring at 75-80° C. The eruption of red-hot flame indicated the formation of cobalt ferrite particles after approximately 5 hours. The CoF particles were then calcined at 600° C in a muffle furnace for

6 hrs. Following calcination, the particles were ground to fine powder using mortar pestle and subsequently stored for further use.

$$9\ Co(NO_3)_2.6H_2O + 18\ Fe(NO_3)_3.9H_2O + 40\ C_2H_5NO_2 = 9\ CoFe_2O_4 + 316\ H_2O + 80\ CO_2 + 56\ N_2 \quad (3.2)$$

Copper ferrite ($CuFe_2O_4$) was synthesized by following a chemical reaction (3.3). Initially, 0.0125 mol of $Cu(NO_3)_2$ and 0.025 mol of $Fe(NO_3)_3$ were mixed in 400 mL of double distilled water with continuous stirring on a magnetic stirrer. 0.057 mol of glycine was then added, followed by further stirring and heating at 80 °C. After 6 h, with a sudden burst of flame, copper ferrite particles were obtained. These particles were then calcined in a muffle furnace at 600 °C for 5 hours. Finally, the particles were ground to fine powder in a mortar pestle and stored for further use.

$$9\ Cu(NO_3)_2.3H_2O + 18\ Fe(NO_3)_3.9H_2O + 40\ C_2H_5NO_2 = 9\ CuFe_2O_4 + 289\ H_2O + 80\ CO_2 + 56\ N_2 \quad (3.3)$$

Combustion synthesis process is highly exothermic in nature. It is crucial to maintain the temperature of the hot plate/magnetic stirrer below 100 °C to prevent excessive gas generation that could lead to material ejection. Slow and steady combustion process must be followed while prioritizing safety measures by maintaining a safe distance from the combustion setup and using appropriate safety gears. A schematic diagram, laboratory set-up, and flow diagram for the synthesis of binary metal-oxides has been presented in figure 3.3.

(a)

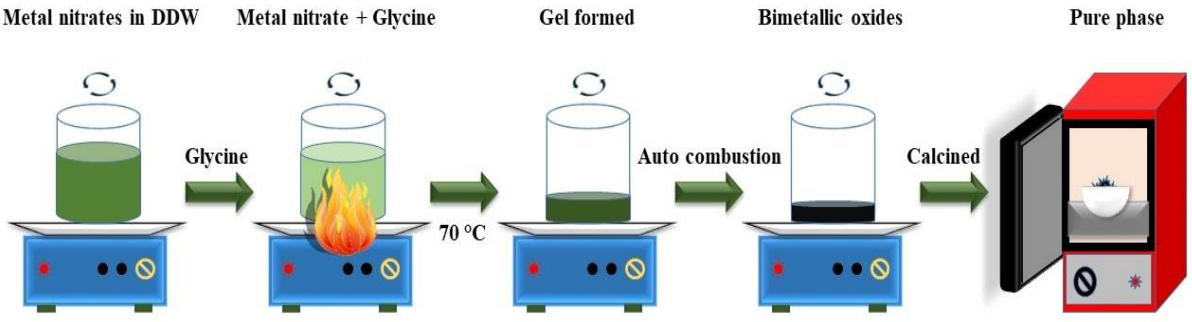

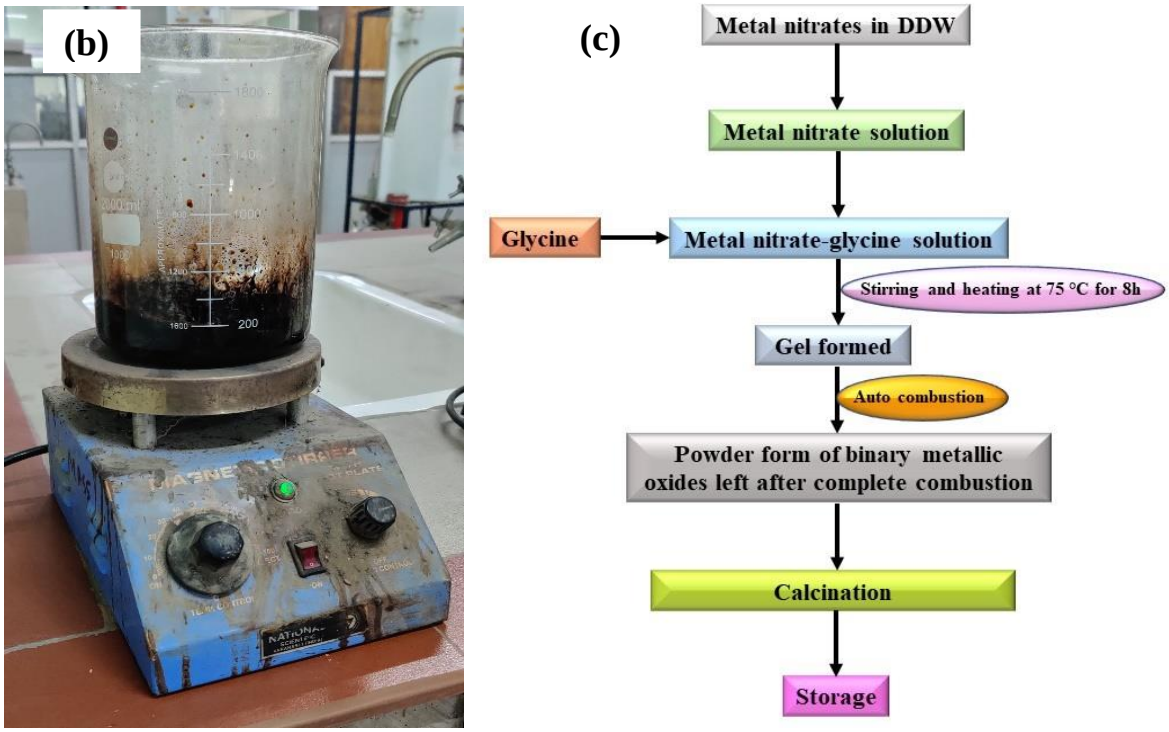

Fig 3.3: (a) Schematic diagram, (b) laboratory set-up, and (c) flow-diagram for the synthesis of binary metal oxides

3.4 Synthesis of activated carbon (AC)

The AC used in the study was prepared from waste coconut shells obtained from nearby temples of the IIT-BHU Varanasi campus. The collected shells were collected carefully and underwent a thorough washing process with double-distilled water to remove any adherent dust and impurities. Subsequently, the shells were dried overnight at 105 °C then ground to a fine powder. The material was then carbonized at 500° C for 1 hour under an inert atmosphere (N_2) in a cylindrical lab-based reactor. The biochar thus obtained was then activated by soaking in 1 M KOH solution. The activation process further involved subjecting the biochar to thermal treatment at three different temperatures, 600 °C, 700 °C and 800 °C under inert atmosphere [213]. The resulting activated carbons were named as AC_1, AC_2, and AC_3 respectively. The obtained activated carbon materials were then washed thoroughly with 1 M HCl solution followed by washing with double distilled water until the pH reached neutral level. The heating

rate used during thermal activation was 15 °C/min and a N_2 flowrate of 100 mL/min was maintained. The proximate analysis results of the coconut shell powder are: fixed carbon- 14.38 %, volatile matter-79.0, moisture-5.7 %, and ash 0.92 %.

To determine the most suitable AC material among AC_1, AC_2, and AC_3, cyclic voltametric experiments were performed at a scan rate of 1 mV/s. Among these samples, AC_3 exhibited the highest specific capacitance of 219 F/g surpassing the values of 177 F/g and 196 F/g for AC_1 and AC_2, respectively (Figure A6 - appendix). Based on this superior performance, AC_3 was selected for further use in synthesis of binary and ternary composite materials and termed as AC hereafter. It is worth mentioning that, AC possesses a BET surface area of 489 m^2/g (Fig. A2 (B) - appendix) indicating its favourable porosity for electrochemical applications. A flow diagram and laboratory-set illustrating the synthesis of AC has been shown in figure 3.4 (a) and (b), respectively.

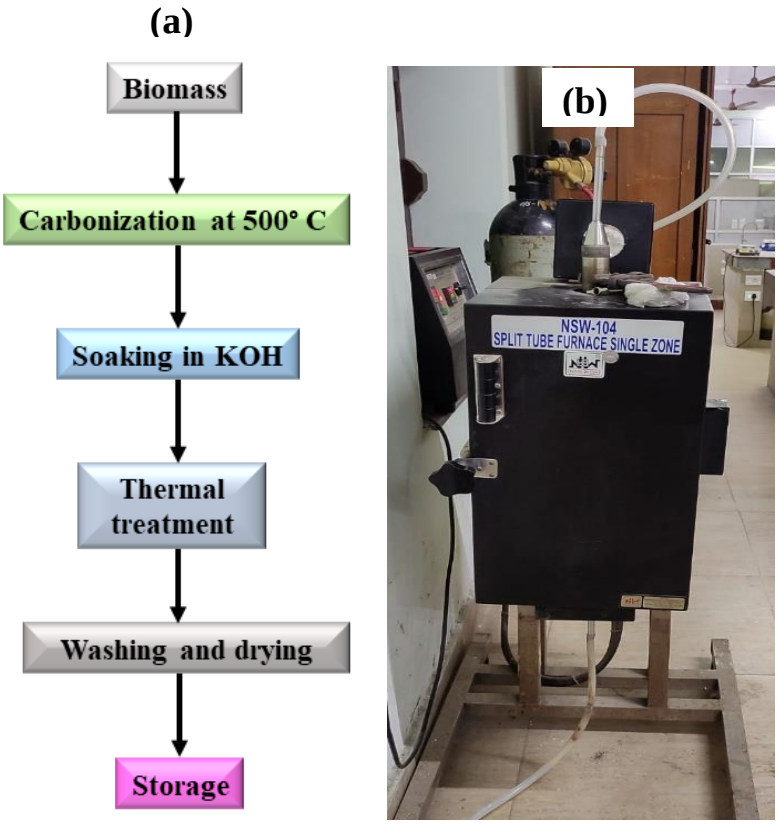

Fig 3.4: (a) Flow diagram and (b) laboratory reactor set-up for synthesis of AC

3.5 Synthesis of binary composite materials

For, PANI/AC, a suspension of AC suspension was prepared by adding 2.30 g of AC in 50 mL DDW. The suspension was added to the PTSA-aniline solution before the drop-by-drop addition of the APS solution. A procedure similar to PANI was then followed to prepare the PANI/AC binary composite. The mass ratio of aniline monomer (AN) to activated carbon was kept at 4:1.

For PANI/CuCo binary composite, 2.30 g suspension of CuCo in 50 mL DDW was added to the PTSA-aniline solution. Drop by drop addition of APS was started, and the subsequent steps of PANI was followed to get the binary composite. The mass ratio of aniline monomer (AN) to CuCo maintained at 4:1.

Similarly, for PANI/CoFe binary composite, 2.30 g suspension of CoFe in 50 mL DDW was added to the PTSA-aniline solution. Drop by drop addition of APS was started, and the remaining procedure of PANI was followed to get the binary composite. The mass ratio of aniline monomer (AN) to CoFe was maintained at 4:1.

For PANI/CuFe binary composite, 2.30 g suspension of CuFe in 25 mL DDW was added to the PTSA-aniline solution. Drop by drop addition of APS was initiated, and the rest of the procedure of PANI synthesis was followed to get the binary composite. The mass ratio of aniline monomer (AN) to CuFe was maintained at 4:1.

A flow-diagram for the synthesis of binary composite materials has been shown in figure 3.5. The experimental details for the synthesis of prepared binary composite materials have been compiled in Table 3.2.

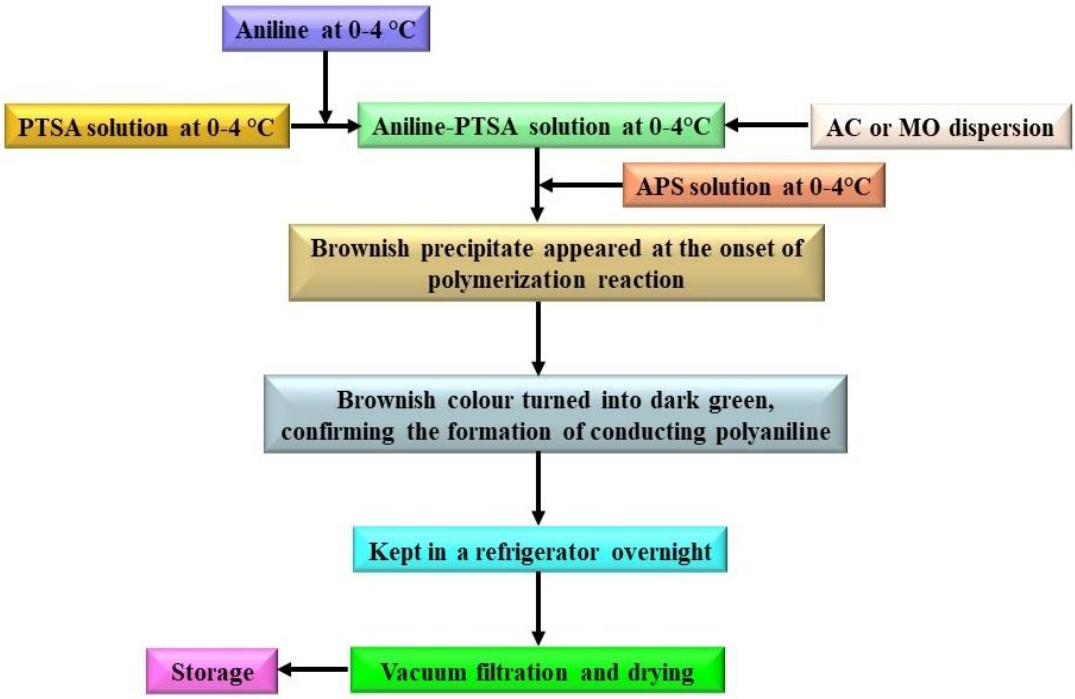

Fig 3.5: Flow-diagram for the synthesis of binary composite materials

Table 3.2: Experimental details of the synthesis of binary composites

Sample name	Participating materials	Weight ratio of AN:AC or AN:MO	Quantity of materials (mL or g)
PANI/AC	Polyaniline and activated carbon	4:1	AN = 9.12 mL AC = 2.325 g
PANI/CuCo	Polyaniline and copper cobaltite	4:1	AN = 9.12 mL CuCo = 2.325 g
PANI/CoFe	Polyaniline and cobalt ferrite	4:1	AN = 9.12 mL CoFe = 2.325 g
PANI/CuFe	Polyaniline and copper ferrite	4:1	AN = 9.12 mL CuFe = 2.325 g

3.6 Synthesis of ternary composite materials

For the preparation of ternary composites, a similar process as for binary composites was followed.

For PANI/AC/CuCo ternary composite, 2.30 g suspension of AC and CuCo each was prepared in 50 mL DDW and added to the PTSA-aniline solution. Drop by drop addition of APS was initiated, followed by the remaining steps of PANI synthesis for binary composites. The mass ratio of aniline monomer (AN) to AC to CuCo was maintained at 4:1:1.

Similarly, for PANI/AC/CoFe ternary composite, 2.30 g suspension of AC and 2.3 g suspension of CoFe was prepared separately in 50 mL DDW. These suspensions were added to the PTSA-aniline solution Drop by drop addition of APS was started, and the rest of the procedure of PANI synthesis was followed. The mass ratio of aniline monomer (AN) to AC to CoFe was maintained at 4:1:1.

For the PANI/AC/CuFe ternary composite, 2.30 g suspension of AC and CuFe each was prepared in 50 mL DDW. The suspensions were added to the PTSA-aniline solution. Drop by drop addition of APS was started, and the subsequent steps of PANI synthesis was followed to get the ternary composite. The mass ratio of aniline monomer (AN) to AC to CuFe was maintained at 4:1:1 in the ternary composite.

A flow-diagram for the synthesis of binary composite materials has been shown in figure 3.6. Table 3.3 provides the experimental details for the synthesis of ternary composite materials.

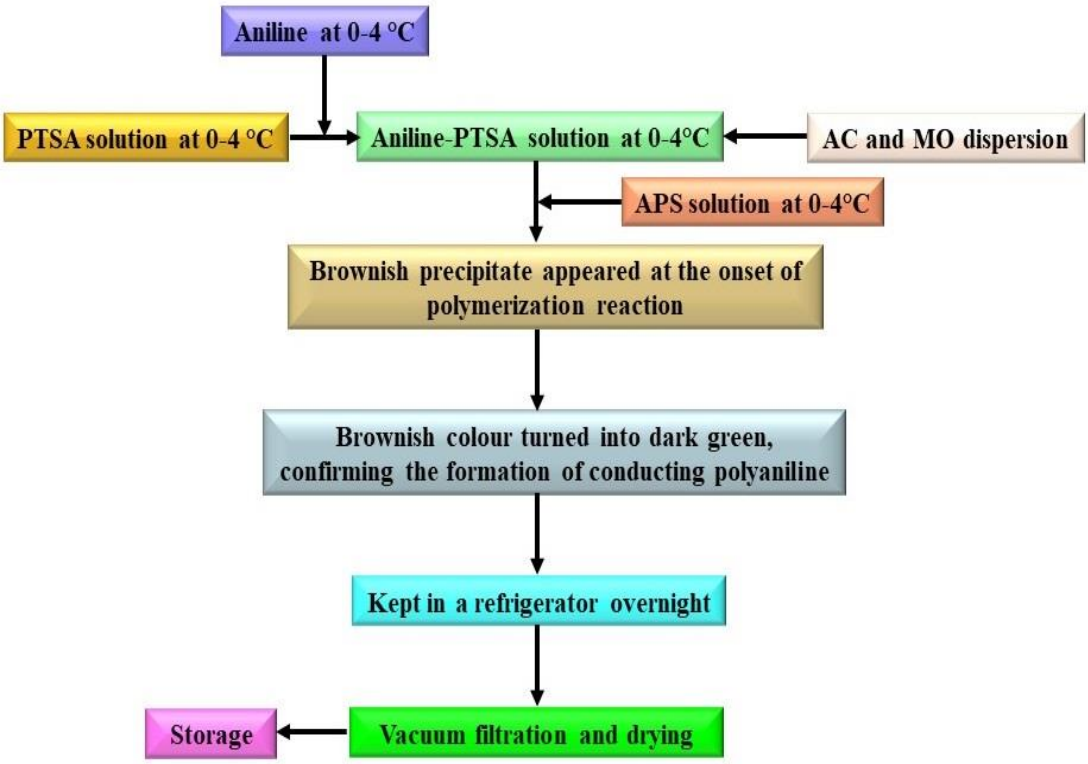

Fig 3.6: Flow-diagram for the synthesis of ternary composite materials

Table 3.3: Experimental details for the synthesis of ternary composites

Sample name	Participating materials	Weight ratio of AN:AC:MO	Quantity of materials (mL or g)
PANI/AC/CuCo	Polyaniline, activated carbon and copper cobaltite	4:1:1	AN = 9.12 mL AC = 2.325 g CuCo = 2.325 g
PANI/AC/CoFe	Polyaniline, activated carbon and cobalt ferrite	4:1:1	AN = 9.12 mL AC = 2.325 g CoFe = 2.325 g

PANI/AC/CuFe	Polyaniline, activated carbon and copper ferrite	4:1:1	AN = 9.12 mL AC = 2.325 g CuFe = 2.325 g

3.7 Fabrication of supercapacitor electrodes

The electrode fabrication process plays an important role in determining the performance of supercapacitor. Careful electrode fabrication is crucial for optimizing the surface area, porosity, distribution, adhesion and interface properties of the electrodes. These factors collectively contribute to improve energy storage capacity, energy and power density, cyclability etc.

As part of the electrode fabrication process, conductive fillers such as carbon black, acetylene black, metal particle, graphite and binders like PTFE, PVDF, SPEEK, Nafion, have been extensively used for preparation of electrodes [210,214]. Supercapacitors endure a significant volume change in their electroactive species during charging and discharging. This can potentially cause detachment of the species from the substrate. However, the binders prevent this detachment, thereby contributing to the extended cycle life of supercapacitor.

In the present study, a copper wire was taken as the current collector. A carbon paper substrate from Toray was attached to the copper wire with the help of silver conductive adhesive paste. Back side of the carbon paper and the exposed portion of the copper wire were insulated by applying hot glue. A dispersion was prepared by mixing 1.7 mg of the synthesized material (active material), 80 µL of 2-propanol and 10 µL Nafion binder. A certain amount of the resulting slurry depending on the desired active mass loading was drop casted on the carbon paper of 1 cm^2 area. The prepared electrodes were dried at room temperature. For experimental setup, symmetric systems consisting of two identical working electrodes (with same mass loading) were used. Whatmann filter paper served as separator in symmetric two-electrode

device. Figure 3.7 (a) shows a single supercapacitor electrode and (b) shows a symmetric device comprising two identical electrodes.

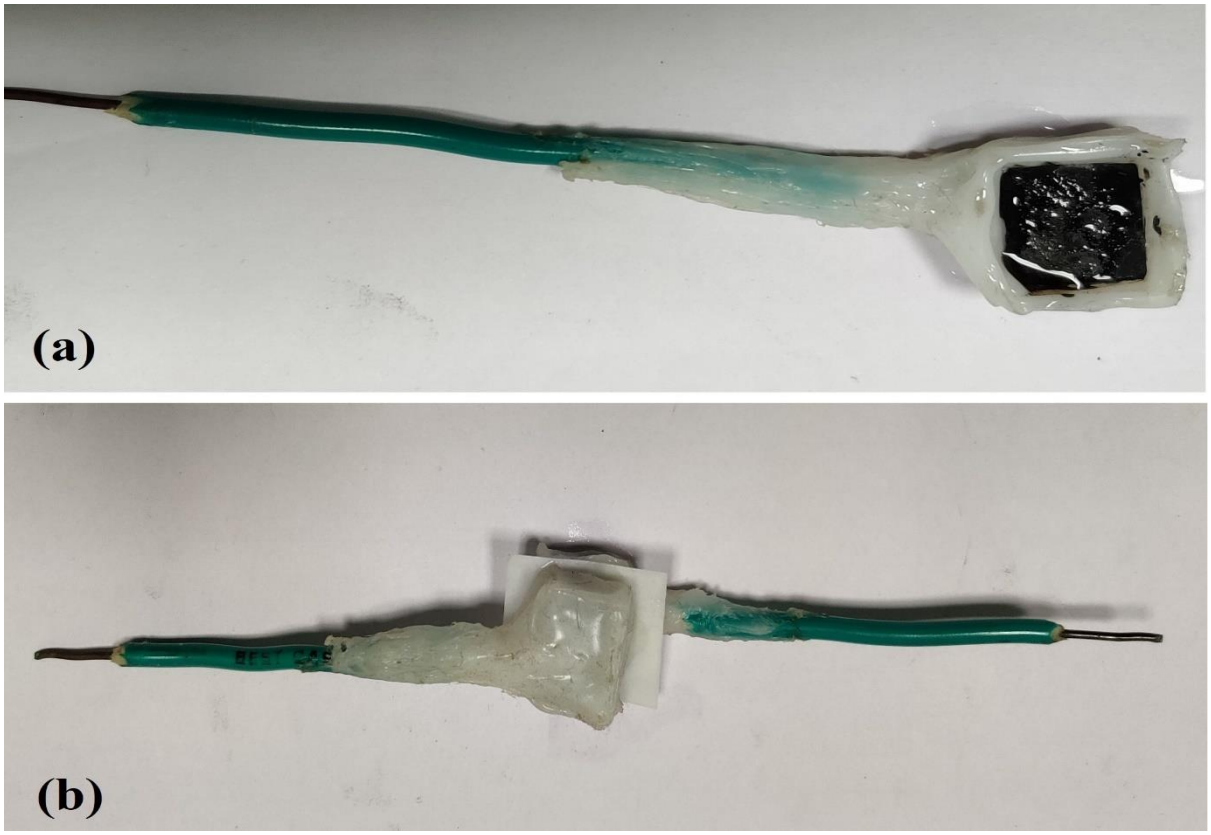

Fig 3.7: (a) a single electrode and (b) a symmetric supercapacitor device

Table 3.4: Characterization techniques used in the present study

S No.	Characterization technique	Characteristics studied
1.	XRD	Phase identification
2.	FTIR	Functional group analysis
3.	XPS	Oxidation states of the elements
4.	FESEM	Surface morphology of the samples
5.	EDS	Elemental analysis
6.	TEM	Inner morphology

7.	BET	Specific surface area of activated carbon sample
8.	CV	Stable potential window determination, voltage-current relation, specific capacitance calculation
9.	CD	Determination of charging and discharging time, specific capacitance, coulombic efficiency, specific energy and power
10.	EIS	Charge transfer resistance, variation of net impedance, admittance, and capacitance with frequency, Knee frequency

3.8 Material characterization

3.8.1 X-ray diffraction (XRD)

X-ray diffraction technique was used to identify the phase of the synthesized samples. XRD patterns of all the samples were obtained by using Cu Kα radiation having wavelength (λ) of 1.54056 Å with the help of an X-ray powder diffractometer (Rigaku Miniflex) in the range of 10° to 80°. The applied current and voltage were 200 mA and 40 kV, respectively. The calculated D-values were matched with the standard data of the corresponding JCPDS files and the existing phases were identified. The crystallite size of the metal oxides was estimated by Scherrer's equation (eq. 3.4) and interlayer spacing was calculated from Bragg's formula (eq. 3.5).

$$\mathbf{D} = \frac{\mathbf{K\lambda}}{\mathbf{\beta_L \cos\theta}} \tag{3.4}$$

$$\mathbf{X = \lambda / 2 \sin \Theta} \tag{3.5}$$

D is the average crystallite size, λ is the X-ray wavelength (1.54056 Å), θ is the Bragg angle. K is the Scherrer's constant (we have taken 0.9 for spherical particle and 0.94 for nanorods).

β_L ($\beta_{exp.}$ - β_I) represents the full width at half maximum in radians, where $\beta_{exp.}$ and β_I are the full width at half maximum of the sample and instrumental broadening, respectively.

3.8.2 Fourier transform infrared spectroscopy (FTIR)

In FTIR, the functional groups are identified depending upon various vibration modes of the respective groups. Each sample was mixed with KBr (binder) to make pellet. Then, FTIR spectra were recorded by Nicolet iS5-Thermo electron scientific instruments LLC spectrophotometer in IR range of 4000-400 cm^{-1} for 64 scans at a resolution of 4 cm^{-1}. The data has been reported in the form of wavenumber vs. transmittance.

3.8.3 X-ray photoelectron spectroscopy (XPS)

XPS provides information about the oxidation states of the elements present in a material. In this technique, X-ray beam is irradiated on a sample, and XPS spectra are recorded by measuring the kinetic energy and analysing the number of electrons which escape from the sample. Soft X-ray Mg Kα is used as a source under ultra-high vacuum. The specimen absorbs photons and electrons are ejected due to photoelectric effect. The ejected electrons have energy of $E_{KE} = h\nu - E_{BE}$, where, E_{KE} is the kinetic energy of ejected electron, E_{BE} is the binding energy of electron and hν is the energy of photon. Each element has a particular binding energy. Therefore, a particular element can be identified by measuring the energy of photoelectron.

In the current study, monochromatic Mg Kα (1253.6 eV) was used as an X-ray source in AMICUS, Kratos Analytical instrument to carry out XPS analysis. 2×10^{-6} kPa of vacuum was maintained inside the analyser chamber.

3.8.4 Field emission scanning electron microscopy (FESEM) and Energy-dispersive X-ray spectroscopy (EDX)

Nova Nano SEM 450 (FEI company of USA (S.E.A) PTE, LTD) was used to study the surface morphology of the synthesized samples by field emission scanning electron microscopy

(FESEM). The instrument was operated under vacuum and voltage of l kV. Various images were captured at different working distances and resolutions to get detailed information about the surface morphology. Team Pegasus Integrated EDX-EBSD with octane plus and Hikari Pro equipped with the FESEM machine was used to determine elemental percentages of the constituents by EDX.

3.8.5 Transmission electron microscopy

Tecnai G2 20 Twin (FEI company of USA (S.E.A) PTE, LTD) was used to conduct transmission electron microscopy (TEM). The instrument was operated under vacuum and voltage of l kV. Different images were captured at different working resolutions to get detailed information about the surface morphology.

3.8.6 BET (Brunauer, Emmett, and Teller) specific surface area analysis

The Brunauer, Emmett, and Teller specific surface area (S_{BET}) of the samples were evaluated by MICROMERITICS-ASAP 2020 surface area and pore size analyser. Low temperature N_2 adsorption-desorption isotherms were carried out at -196 °C. N_2 gas is physically adsorbed on the sample surface and form monomolecular layer on its surface.

3.9 Electrochemical characterization & performance evaluation

The performances of the supercapacitor electrodes were assessed using various electrochemical techniques like cyclic voltammetry (CV), charge-discharge (CD), and electrochemical impedance spectroscopy (EIS). Specific capacitance (F/g), energy density (Wh/kg), power density (W/kg), coulombic efficiency (%), cycle life (% retention), impedance are the factors which determine the efficacy of electrochemical supercapacitors and supercapacitor electrodes.

Various types of electrodes are used in the electrochemical measurements, such as, working electrode (WE), sense electrode (SE), reference electrode (RE), counter electrode (CE), and ground electrode (GE). The VersaSTAT3 instrument was used for all the electrochemical

measurements. The working electrode is the electrode where the relevant electrochemical reactions occur. Sense electrode is connected to the working electrode, and it controls the voltage in between the reference electrode and itself. Similarly, the voltage between reference electrode and sense electrode is measured by reference electrode. The role of counter electrode is to control the VersaSTAT3 power output. Ground lead provides ground point in the electrochemical cell, acts as a Faraday shield, and safeguards the set up during any surge of excessive electrical charges. Further, all the electrochemical characterizations were conducted at 25° C.

In three electrode systems, Ag/AgCl, Platinum, and active (synthesized) material-based electrode is taken as reference, counter, and working electrode, respectively. In two electrode systems, the reference and counter leads are connected to one electrode of the supercapacitor, while the other electrode is connected to working and sense electrode lead. The desired electrical connections of three and two electrode systems have been shown in figure 3.8 (a) and (b). A schematic illustration of electrochemical workstation set-up and laboratory set-up has been demonstrated in figure 3.9 (a) and (b).

Note: During the electrochemical characterizations, the working electrode potential is measured relative to the reference electrode (here, Ag/AgCl) and the counter electrode (here, platinum) is employed to complete the electrical circuit through which current flows.

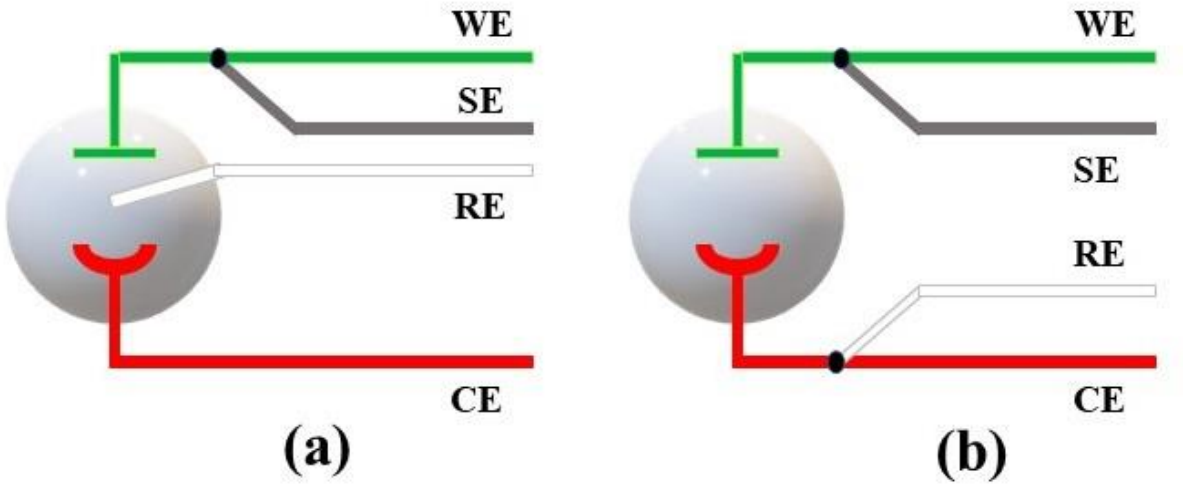

Fig 3.8: (a) Three electrode and (b) two electrode cell configurations

(a)

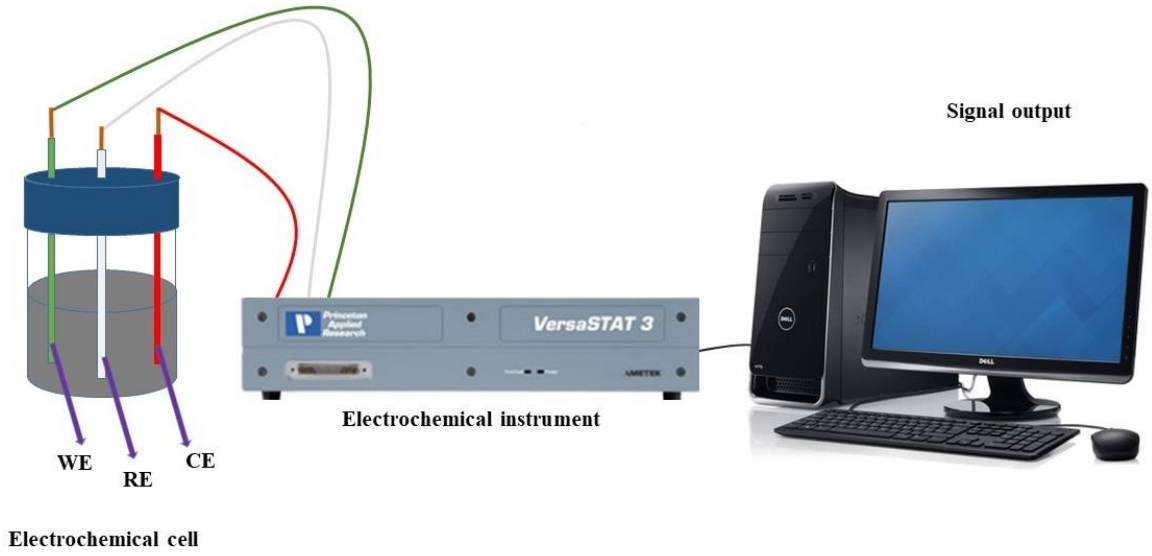

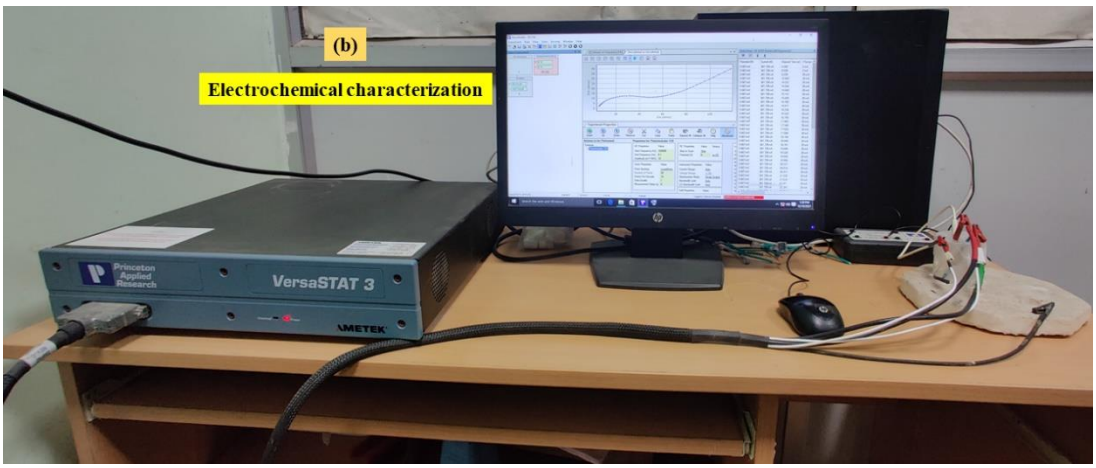

Fig 3.9: (a) Schematic diagram of experimental set-up, (b) experimental set-up used in the laboratory for electrochemical characterization

3.9.1 Cyclic voltammetry (CV)

Cyclic voltammetry is a potentiodynamic electrochemical technique that involves applying a potential within the stabile potential window of the system at a particular scan rate. Current is generated based on the conductivity of the material used in the working electrode. The forward (anodic) and backward (cathodic) scan complete a cycle and the trace is known as cyclic voltammetry curve. The potential is applied between working and reference electrode, while the current is measured between working and counter electrode.

EDLC based materials like activated carbon, CNT, graphene oxide, etc. exhibit rectangular type CV curve. On the other hand, pseudocapacitive materials like metal oxides (MnO_2, RuO_2, $CuCo_2O_4$, $CoFe_2O_4$, etc.), and conducting polymers (polyaniline, polythiophene, polypyrrole, etc.) exhibit redox transitions. Typically, the CV curve has two regimes: capacitive regime dominated by double layer formation, and a faradaic regime that is prevailed by faradaic reactions [215,216].

The CV plot of an ideal capacitor is rectangular in shape. However, the deviation from rectangular shape in EDLC and pseudocapacitive material-based supercapacitor can be attributed to the presence of functional groups and redox transitions, respectively [217,218]. In composite material-based supercapacitors, both the EDLC and pseudocapacitive materials may contribute significantly to get an enhanced electrochemical property. The specific capacitance, which quantifies the charge storage capacity can be calculated using the following formulae (eq 3.5, 3.6 and 3.7).

Specific capacitance from CV

$$\mathbf{C_{sp,ele}} = \frac{\int \mathbf{I}\,.\,\mathbf{dV}}{\mathbf{m_{ele}}.\ \boldsymbol{\nu}\,.\,\Delta\mathbf{V}} \tag{3.6}$$

$\mathbf{C_{sp,ele}}$ = Specific capacitance of a single electrode in Farad per gram (F/g)

$\int \mathbf{I.\,dV}$ = Area under the cathodic scan in Ampere.Volt (AV)

$\mathbf{m_{ele}}$ = mass of the active material in gram (g)

$\boldsymbol{\nu}$ = Potential scan rate in volt per second (V/s)

$\Delta\mathbf{V}$ = Stability potential window in volt (V)

Equation 3.5 can also be written as:

$$\mathbf{C_{sp,ele}} = \frac{\int \mathbf{I}\,.\,\mathbf{dV}}{\mathbf{2}\,.\,\mathbf{m_{ele}}\,.\,\boldsymbol{\nu}\,.\,\Delta\mathbf{V}} \tag{3.7}$$

In equation 3.6, $\int \mathbf{I.}\,\mathrm{dV}$ is the area under the whole CV curve. Factor '1/2' is included so as to correctly calculate the specific capacitance without overestimating the values.

Likewise,

$$\mathbf{C_{sp,sup}} = \frac{\int \mathbf{I}\,.\,\mathbf{dV}}{\mathbf{m_{tot}}\,.\,\boldsymbol{\nu}\,.\,\Delta\mathbf{V}} \tag{3.8}$$

$\mathbf{C_{sp,sup}}$ = Specific capacitance of the supercapacitor (F/g)

$\int \mathbf{I.\,dV}$ = Area under the cathodic scan (AV)

$\mathbf{m_{tot}}$ = total mass of the active material (g) = $\mathbf{m_{positive\ electrode}}$ $(\mathbf{m_{pe}})$+ $\mathbf{m_{negative\ electrode}}$ $\mathbf{(m_{ne})}$

3.9.2 Charge-discharge (CD)

In charging-discharging (CD) technique, a constant current is applied during the process and the change in voltage of the supercapacitor with time is recorded. This is the most efficient

technique for evaluation of capacitance. In EDLC, the potential window range is not restricted to a particular value as the charge storage is independent of potential. However, for simple faradaic and intercalated pseudocapacitors, the range of potential window is fixed. In general, the CD plots of EDLCs exhibit a linear and triangular in shape, whereas for pseudocapacitors we get distorted CD plots with significant or negligible voltage drop. The charging and discharging time represent the response of a supercapacitor during any operation. The CD plot of an ideal capacitor is triangular in nature. But one may observe deviation from triangular shape due to the presence functional groups in EDLC and redox reactions in pseudocapacitors. In case of composite systems, the deviation appears due to the presence of both type materials (EDLC and pseudocapacitive).

Specific capacitance can be calculated from the data obtained in CD.

$$\mathbf{C_{sp,ele}} = \frac{\mathbf{I}\,.\,\mathbf{t_d}}{\mathbf{m_{ele}}\,.\,\Delta\mathbf{V}} \tag{3.9}$$

I = Discharging current (A)

t_d = Discharging time (s)

Likewise,

$$\mathbf{C_{sp,sup}} = \frac{\mathbf{I}\,.\,\mathbf{t_d}}{\mathbf{m_{tot}}\,.\,\Delta\mathbf{V}} \tag{3.10}$$

There are various expressions for different types of configurations. For two equivalent electrodes having same capacitance and weight (symmetric systems), $\mathbf{C_{positive}} = \mathbf{C_{negative}}$.

$C_{positive}$ (C_{pe}) = Capacitance of positive electrode (pe)

$C_{negative}$ (C_{ne}) = Capacitance of negative electrode (ne)

The positive and negative electrodes of supercapacitors are considered to be in series connections with each other.

$$\frac{1}{C_{sup}} = \frac{1}{C_{pe}} + \frac{1}{C_{ne}} \quad (3.11)$$

C_{sup} = Capacitance of supercapacitor in Farad (F)

The charges in the positive and negative electrodes of the supercapacitors should be balanced. Thus,

$$q_{electrode} = m_{pe}.\Delta V_{pe}.C_{sp,pe} = m_{ne}.\Delta V_{ne}.C_{sp,ne} \quad (3.12)$$

$q_{electrode}$ (q_{ele})= Charge in the electrode in coulombs

m_{pe} = Active mass on positive electrode (g)

ΔV_{pe} = Potential window of positive electrode (V)

$C_{sp,pe}$ = Specific capacitance of positive electrode (F/g)

m_{ne} = Active mass on negative electrode (g)

ΔV_{ne} = Potential window of negative electrode (V)

$C_{sp,ne}$ = Specific capacitance of negative electrode (F/g)

For symmetric configurations,

$C_{pe} = C_{ne} = C_{electrode}$

$C_{electrode}$ (C_{ele}) = Capacitance of each electrode (F)

Equation 3.10 becomes,

$$C_{sup} = \frac{1}{2}.C_{ele} \quad (3.13)$$

$$C_{sp,sup} = \frac{C_{sup}}{m_{tot}} = \frac{C_{ele}}{2} \cdot \frac{1}{2m_{ele}} = \frac{C_{sp,ele}}{4} \quad (3.14)$$

For electrodes having Cpe ≠ Cne, the expressions are as follows.

From equation 3.11,

$$C_{sp,pe} = \frac{m_{ne} \cdot \Delta V_{ne} \cdot C_{sp,ne}}{m_{pe} \cdot \Delta V_{pe}} \quad (3.15)$$

$$C_{sp,ne} = \frac{m_{pe} \cdot \Delta V_{pe} \cdot C_{sp,pe}}{m_{ne} \cdot \Delta V_{ne}} \quad (3.16)$$

Dividing equation 3.10 by m_{tot} ,

$$C_{sp,sup} = \frac{1}{m_{tot}} \cdot \frac{C_{ne} \cdot C_{pe}}{C_{ne} + C_{pe}}$$

$$= \frac{1}{m_{tot}} \cdot \frac{C_{sp,ne} \cdot C_{sp,pe}}{\frac{C_{sp,ne}}{m_{pe}} + \frac{C_{sp,pe}}{m_{ne}}}$$ (Dividing numerator and denominator by $m_{pe} \cdot m_{ne}$)

$$= \frac{m_{ne} \cdot m_{pe}}{m_{tot}} \cdot \frac{C_{sp,ne} \cdot C_{sp,pe}}{C_{sp,ne} \cdot m_{ne} + C_{sp,pe} \cdot m_{pe}}$$

$$= \frac{m_{ne} \cdot m_{pe}}{m_{tot}} \cdot \frac{C_{sp,ne} \cdot m_{ne} \cdot \Delta V_{ne} \cdot C_{sp,ne}}{m_{pe} \cdot \Delta V_{pe} \cdot \left(C_{sp,ne} \cdot m_{ne} + \frac{m_{ne} \cdot \Delta V_{ne} \cdot C_{sp,ne}}{m_{pe} \cdot \Delta V_{pe}} \cdot m_{pe}\right)}$$ (Replacing $C_{sp,pe}$ as per equation 3.14)

$$= \frac{C_{sp,ne} \cdot m_{ne} \cdot \Delta V_{ne}}{m_{tot} \cdot \Delta V_{pe} \cdot \left(1 + \frac{\Delta V_{ne}}{\Delta V_{pe}}\right)} = \frac{m_{ne}}{m_{pe} + m_{ne}} \cdot C_{sp,ne} \cdot \frac{\Delta V_{ne}}{\Delta V_{ne} + \Delta V_{pe}}$$

$$C_{sp,ne} = C_{sp,sup} \cdot \frac{m_{ne} + m_{pe}}{m_{ne}} \cdot \frac{\Delta V_{ne} + \Delta V_{pe}}{\Delta V_{ne}} \quad (3.17)$$

Similarly,

$$C_{sp,pe} = C_{sp,sup} \times \frac{m_{pe} + m_{ne}}{m_{pe}} \times \frac{\Delta V_{pe} + \Delta V_{ne}}{\Delta V_{pe}} \quad (3.18)$$

Specific energy and power

Energy density is the amount of charge a supercapacitor can hold. It is directly proportional to the capacitance and square of the potential difference between the supercapacitor electrodes.

Equation for specific energy,

$$E_{sp,sup} = \frac{1}{2} \cdot C_{sp,sup} \cdot (\Delta V)^2 \quad (3.19)$$

$E_{sp,sup}$ = Specific energy of the supercapacitor in Watt-hour per kilogram (Wh/kg)

Power density is the rate at which a device delivers the stored energy during an application.

$$P_{sp,sup} = \frac{E_{sp,sup}}{t_d} \quad (3.20)$$

$P_{sp,sup}$ = Specific power of the supercapacitor (W/kg)

t_d = Discharging time of the supercapacitor (s)

Note:

Unit conversion of specific energy and power

In general, we know that W = Vq, q = It, and P = VI

W is the work done, V is the voltage, q is charge, I is current, t is time, and P is the power.

So, W = VIt = Pt and its unit will be Watt.sec

$\frac{W}{m}$ will have the unit of Watt.sec.g^{-1} (if mass is taken in gram). To convert this into Watt.h.kg^{-1}, $\frac{1}{3.6}$ will be multiplied to Watt.sec.g^{-1}. ESP is nothing but the work done per unit mass ($\frac{W}{m}$). So, to convert the unit the equation will be as follows.

$$\mathbf{E_{sp,sup} = \frac{1}{7.2} . C_{sp,sup} . (\Delta V)^2 \ in\ Wh.kg^{-1}} \quad (3.21)$$

Similarly,

$$\mathbf{P_{sp,sup} = \frac{E_{sp,sup} . 3600}{t_d} \ in\ W.kg^{-1}} \quad (3.22)$$

Coulombic efficiency (η)

Coulombic efficiency demonstrates the efficiency at which charges (electrons) are transferred in an electrochemical system during the operation of the device. It is also called as current efficiency or faradaic efficiency.

$$\mathbf{\eta\ \% = \frac{t_d}{t_c} . 100} \quad (3.23)$$

η % = Percentage coulombic efficiency (CE)

t_d = Discharging time of the supercapacitor (s)

t_c = Charging time of the supercapacitor (s)

Cycle life

The reliability of a supercapacitor is estimated from its percentage retention over repeated cycles of charge-discharge or cyclic voltammetry. Supercapacitors exhibit excellent capacitance retention and higher cycle life than batteries and fuel cells.

3.9.3 Electrochemical impedance spectroscopy (EIS)

Electrical resistance is the opposition encountered by a circuit element to the flow of electrical current. An ideal resistor follows Ohm's law (V=IR) regardless of voltage and current levels. It remains constant across all frequencies, and all the AC voltage and current in such resistors lie in phase with each other. However, in real life applications, the circuit elements display complex behaviour and they do not allow us to implement the general concepts of resistance. To account for this complexity, a more comprehensive term, impedance in employed. Like resistance, impedance is also the measure of the obstruction offered by a circuit element.

In the realm of supercapacitor applications, the impedance is measured by electrochemical impedance spectroscopy (EIS) technique [219–221]. EIS allows for characterization and analysis of the impedance behaviour of supercapacitors, providing valuable insights into their electrochemical performance.

According to Ohm's law,

$V \propto I$

$$\Rightarrow \mathbf{V = IR} \tag{3.24}$$

V is the potential in volt (V), I is the current in Ampere (A), and R is the resistance in Ohm (Ω).

In an electrochemical supercapacitor, an AC potential is applied to measure the electrochemical impedance.

$$\mathbf{V_X = |V_0| \, Sin(\omega t)} \tag{3.25}$$

V_X = Potential at time x (Volt)

V_0 = Amplitude of applied signal (Volt)

ω = Radial frequency (radians/second)

$$\omega = 2\pi f$$

f = Frequency in Hertz (Hz)

$$I_X = |I_0| \, Sin(\omega t + \phi) \tag{3.26}$$

I_X is the response signal (A), ϕ is the phase shift, and I_0 is the amplitude of current.

Applying an analogy of Ohm's law for the calculation of impedance,

$$Z = \frac{V_X}{I_X} = \frac{|V_0| \, Sin(\omega t)}{|I_0| \, Sin(\omega t + \phi)} = |Z_0| . \frac{Sin(\omega t)}{Sin(\omega t + \phi)} \tag{3.27}$$

According to Euler's formula,

exp (jϕ) = Cos ϕ + j sin ϕ

The impedance can be expressed in the form of a complex function.

$$V_X = |V_0| \exp(j\omega t)$$

$$I_X = |I_0| \exp(j\omega t - \phi)$$

$$j = \sqrt{-1}$$

$$Z = |Z_0| \exp(j\phi) = |Z_0| (\cos\phi + j \sin\phi) = |Z_0| \cos\phi + j |Z_0| \sin\phi = Z_{Re} + j Z_{Im}$$

$$|Z| = \sqrt{Z_{Re}^2 + Z_{Im}^2} \tag{3.28}$$

|Z| = Total impedance in Ohms (Ω)

Z_{Re} = Real part of impedance (Ω)

Z_{Im} = Imaginary part of impedance (Ω)

Table 3.5: Various electronic circuit components and their properties

Component	Phase between current and voltage	Relationship between impedance and frequency
Resistor	Current is in phase with voltage	Impedance is frequency independent
Inductor	Current shifts a phase of -90° with respect to voltage	Impedance increases with frequency
Capacitor	Current shifts 90° with respect to voltage	Impedance and frequency are inversely proportional

An AC amplitude is given to the cell during the EIS process over a frequency range of 100 mHz to 1 MHz. Various plots like Nyquist plot (Z_{Re} vs Z_{Im}) and Bode plot (frequency vs |Z|) are obtained from the EIS data. The point at which the extrapolated plot intersects the real axis at high frequency region, is known as equivalent series resistance (R_{eq}). It is the collective resistances of current collector, substrate, electrolyte, etc. The diameter of the semicircle in the Nyquist plot demonstrates charge transfer resistance (R_{Ct}). The absence of any semicircle represents ultralow charge transfer resistance. Less charge transfer resistance value signifies excellent electron and ion mobility, which enhances the charge-discharge rate of the system [222,223].

3.10 Experimental design for optimization of ternary composite materials using RSM

Response Surface Methodolody was applied by using Design-Expert software version – 13 (StateEase Inc., Minnepolis, USA) optimize the ternary composite materials. The Central Composite Design (CCD), which is a standard tool for RSM design was employed to observe the correlation between the independent parameters towards the surface response, which is here the specific capacitance [224]. In this study, the effect of weight percentage of constituents (AC and binary metal oxides) of composite material on specific capacitance exhibited by the respective electrode material was investigated. The independent variables used are the weight percentages of AC and binary metal oxides while keeping the weight percentage of PANI constant to reduce complexity and minimize the number of experiments. The experimental range and levels of independent factors have been shown in Table 3.6.

Table 3.6: The experimental range and levels of respective independent factors for central composite design.

Variable	Name	Unit	Low value	High value
A (Numeric)	AC	weight percentage	1	5
B (Numeric)	Binary metal oxide	weight percentage	1	5

A total of 13 experiments were performed with 8 non-center and 5 center points. The experimental specific capacitance values were determined and unified from the CV curve at the scan rate of 1 mV/s in three-electrode configuration.

Further, regression analysis used to fit the experimental data which yielded a second-order polynomial equation. Then optimum composition obtained was used to validate and characterize the respective composite materials.